optica

Non-invasive monitoring and control in silicon photonics using CMOS integrated electronics

STEFANO GRILLANDA,[1,*,†] MARCO CARMINATI,[1,†] FRANCESCO MORICHETTI,[1] PIETRO CICCARELLA,[1] ANDREA ANNONI,[1] GIORGIO FERRARI,[1] MICHAEL STRAIN,[2] MARC SOREL,[3] MARCO SAMPIETRO,[1] AND ANDREA MELLONI[1]

[1]*Dipartimento di Elettronica, Informazione e Bioingegneria, Politecnico di Milano, 20133 Milano, Italy*

[2]*Institute of Photonics, The University of Strathclyde, Glasgow G4 0NW, UK*

[3]*School of Engineering, University of Glasgow, Glasgow G12 8QQ, UK*

Corresponding author: stefano.grillanda@polimi.it

As photonics moves from the single-device level toward large-scale, integrated, and complex systems on a chip, monitoring, control, and stabilization of the components become critical. We need to monitor a circuit non-invasively and apply a simple, fast, and robust feedback control. Here, we show non-invasive monitoring and feedback control of high-quality-factor silicon (Si) photonic resonators assisted by a transparent detector that is directly integrated inside the cavity. Control operations are entirely managed by a CMOS microelectronic circuit that is bridged to the Si photonic chip and hosts many parallel electronic readout channels. Advanced functionalities, such as wavelength tuning, locking, labeling, and swapping, are demonstrated. The non-invasive nature of the transparent monitor and the scalability of the CMOS readout system offer a viable solution for the control of arbitrarily reconfigurable photonic integrated circuits aggregating many components on a single chip.   © 2014 Optical Society of America

1. INTRODUCTION

The level of complexity achieved by today's integrated electronic systems is commonly perceived as the result, primarily, of challenging technological efforts to scale device dimensions down to their ultimate physical limits [1]. Although this is indeed true, it is only partially responsible for their success, as miniaturization is not synonymous with large-scale integration. In fact, analog electronic circuits cannot function properly without adequate tools to dynamically steer and hold each embedded device to the desired working point, counteracting functional drifts due to fluctuations in the environment, aging effects, mutual crosstalk, and fault events [2].

This argument is equally applicable to photonic technologies. Even though photonic platforms, like silicon-on-insulator (SOI), have demonstrated maturity for squeezing several

thousands of photonic elements in a footprint of less than 1 mm² [3], the evolution of integrated photonics from device-level to large-scale systems is still a challenge. In fact, when aggregating several components on a single chip, the aforementioned parasitic effects become critical and need to be addressed through feedback control loops that locally monitor and continuously set each optical element to the desired functionality [4].

These issues are particularly severe in silicon (Si) photonic microresonators, due to their extreme sensitivity to fabrication tolerances [5] and temperature variations [6]. Several approaches have recently been proposed to lock the resonant wavelength of Si microrings, for instance by applying dithering signals [7] or homodyne detection schemes [8], and by monitoring the power level [9,10] or bit-error rate [11] of

the optical signal. However, all the techniques proposed so far require the use of on-chip or external photodetectors to partially tap the light travelling in the resonator. Though effective on single devices, this approach is not scalable to large-scale integration circuits [12], where multipoint light tapping would result in a large amount of optical power being wasted for monitoring operation. Local feedback control assisted by transparent optical detectors is envisioned as an enabling tool for the realization of complex and arbitrarily reconfigurable systems on a chip [13–15].

Here, we show a Si photonic–electronic integrated platform enabling the feedback control of Si photonic integrated circuits without the need of tapping any photon from the waveguide. The status of high-quality-factor resonators is monitored by a recently pioneered ContactLess Integrated Photonic Probe (CLIPP) [16] that realizes a fully transparent detector and can be integrated directly inside any photonic circuit, including microrings. The feedback loop, combining the CLIPP readout system and the microring control functions, is entirely integrated onto an electronic CMOS circuit [17] that is wirebonded to the Si photonic chip. Advanced functionalities and control operations such as wavelength tuning, locking, labeling, and swapping are demonstrated in a thermally actuated resonator, proving that the presented Si photonic–electronic integrated platform is an efficient and flexible solution for the realization and control of Si photonic circuits hosting many components.

2. CLIPP CONCEPT AND FABRICATION

Figure 1(a) shows a top-view photograph of a microring fabricated using SOI technology, where the CLIPP electrodes and the thermal actuator are integrated. The microring is 516 μm long, has 20 μm bending radius, and is realized by a channel waveguide with 480 nm wide and 220 nm thick Si core [Fig. 1(b)], patterned by means of electron-beam lithography [18]. The waveguide core is buried into a 1 μm thick silicon dioxide (SiO_2) top cladding that is grown by plasma-enhanced chemical vapor deposition [16,18]. On top of it, the metallic

NiCr heaters and Au pads of the CLIPP are patterned by lift-off technique and placed at sufficient distance from the Si core to avoid any significant interaction with the optical mode.

The CLIPP is constituted simply by two 100 μm long metal electrodes placed on top of the microring waveguide, here mutually spaced by about 83 μm on the side of the bus-to-ring directional coupler. The CLIPP can be fabricated using any CMOS-compatible metal technology, and can exploit traditional processes used for the fabrication of thermal actuators, without requiring any additional or specific process step.

The equivalent electrical circuit of the CLIPP is reported in Fig. 1(c), which shows the longitudinal profile of the waveguide. Due to the typical doping of SOI wafers (10^{15} cm^{-3}, p-type), the Si core acts mainly as a resistor of conductance G, whereas the insulating top cladding provides the access capacitances C_A. The CLIPP monitors variations of the waveguide electric conductance ΔG with optical power P that are induced by a carrier generation effect, occurring at the native Si/SiO_2 interface, associated with intrinsic surface state absorption (SSA) processes [16,19]. These phenomena exist even in ideally smooth interfaces due to the termination of the Si lattice at the walls of the waveguide core [20]. The results shown in this work demonstrate indeed that the CLIPP approach successfully applies to low-loss Si waveguides with a very good quality of the Si/SiO_2 interface. In our waveguides, exhibiting optical loss lower than 1.5 dB/cm, the CLIPP signal-to-noise ratio (SNR) achieved by using low-noise standard CMOS readout electronics (see Section 3) is sufficiently large to make it exploitable for monitoring and feedback control operations (see Sections 4 and 5). This also implies that no specific damaging treatments need to be applied to the waveguide in order to increase the density of interface states, and hence the SNR.

Other all-silicon detectors, based on SSA [19,21] or defect mediated absorption [9,22,23], require the photogenerated carriers to be swept away from the waveguide through highly doped regions or electric lines directly contacted to the Si core, thus resulting in additional optical loss. In contrast, the capacitively coupled electrodes of the CLIPP perform a remote monitoring of the optical field, thus avoiding any perturbation [16]. In this sense, the CLIPP realizes a transparent detector that can be placed in any point of the circuit to monitor its local status without affecting its functionality.

3. CLIPP READOUT SYSTEM

The CLIPP observes directly the amount of light stored in the resonant cavity, information that traditionally is not available unless a portion of the optical power is tapped and rerouted to a photodetector, by measuring variations of the electric conductance G of the waveguide core [16].

Readout operations of the CLIPP electric signal, as well as microring control functionalities (such as wavelength tuning, locking, labeling, and swapping), are performed by means of a custom microelectronic circuit [17] whose schematic is shown in Fig. 2(a). One of the CLIPP electrodes is excited with a sinusoidal electrical signal with frequency f_e and amplitude V_e, whereas the current flow i_e at the other one is collected by means
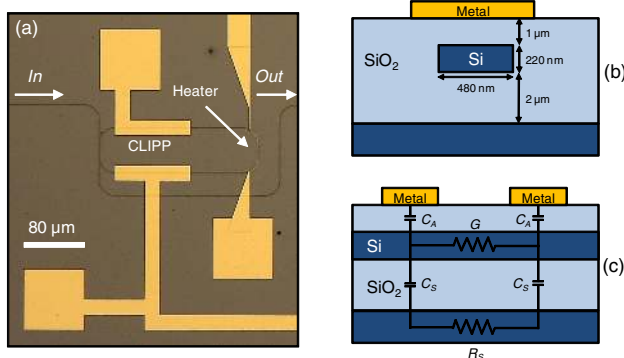

Fig. 1. (a) Top-view photograph of the fabricated Si microring, where CLIPP and thermal actuator are integrated. (b) Cross-section of the Si core waveguide, with the CLIPP metal electrode deposited on top of the SiO_2 cladding. (c) Longitudinal profile of the Si waveguide showing the CLIPP equivalent circuit in the electrical domain. The substrate resistance R_S is negligible with respect to the other impedances of the circuit.
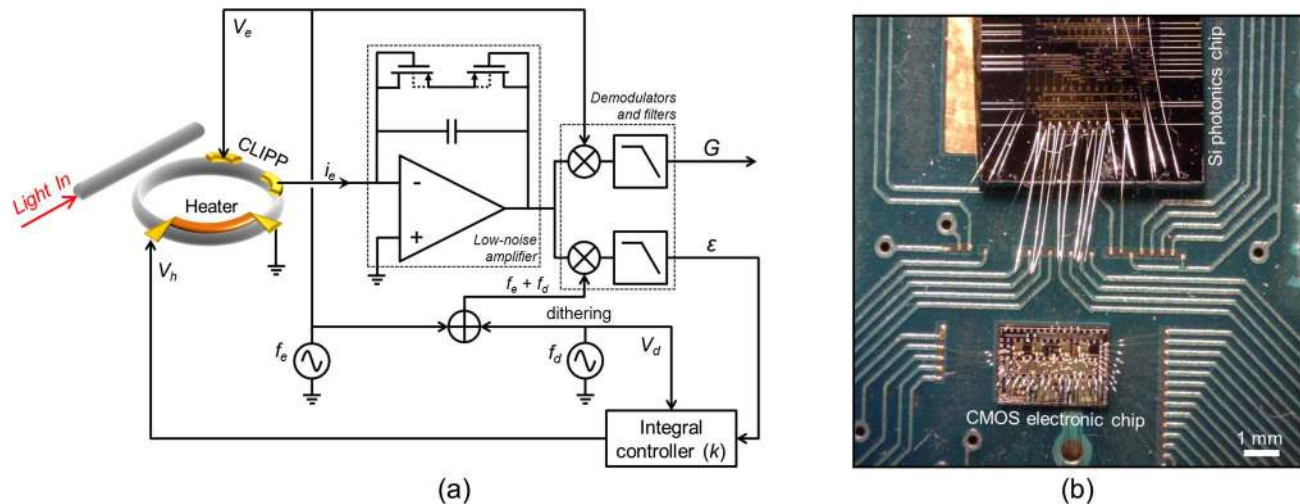
Fig. 2. (a) Schematic of the electronic integrated circuit that performs the readout of the CLIPP electric signal and manages control operations of the Si photonic microring resonator (such as wavelength tuning, locking, labeling, and swapping). (b) Photograph of the Si photonic chip (on the top) hosting the microring resonator that is wire-bonded to the CMOS electronic chip (in the bottom) containing all the CLIPP readout and microring control circuitry. Both the photonic and electronic chips are integrated onto the same printed circuit board.

of a low-noise amplifier. Then, the CLIPP signal is demodulated at frequency f_e to provide the electric conductance G.

The electric readout frequency of the CLIPP is typically around $f_e = 1$ MHz in order to bypass the capacitances C_A and access directly the waveguide conductance G. Actually, as shown in Fig. 1(c), there is a parasitic path composed of stray capacitances C_S across the SiO_2 undercladding and the Si substrate resistance R_S. Due to the Si conductivity and the large thickness of the chip substrate, R_S is negligible compared to the other impedances of the circuit. In this device, C_S is smaller than C_A so that, when the CLIPP is driven at f_e, no significant stray current is injected through the parasitic path that can therefore be neglected.

The amplitude of the applied signal is usually $V_e = 1$ V, so that neither attenuation nor significant perturbation of the optical mode and quality factor is induced [16]. The integrated electronic circuit manages control operations of the microring, like wavelength tuning, locking, labeling, and swapping, using the dithering and feedback controller units reported in the schematic (see Sections 4–6).

The electronic readout circuit is integrated in a CMOS chip (0.35 µm process by AMS Foundry) with 32 readout channels that is wire-bonded to the Si photonic chip hosting the microring resonator (fabricated by the James Watt Nanofabrication Centre at University of Glasgow) [Fig. 2(b)]. Both the electronic and the photonic chips are integrated onto the same printed circuit board. The design of the CMOS chip was optimized to achieve a noise level as low as 2 pS rms with a lock-in bandwidth $B_e = 1$ Hz [17]. This photonic–electronic integrated platform also offers a simple and flexible system for the realization and control of large-scale Si photonic-integrated circuits, hosting several components to achieve complex systems on a chip.

The driving frequency f_e and the SNR of the CLIPP signal are the most relevant parameters for the miniaturization of the CLIPP size. With reference to the equivalent electric circuit of Fig. 1(c), a reduction of the electrode spacing would increase G, whereas a reduction of the electrode length would make C_A smaller. Both these actions would result in a higher driving frequency f_e. For instance, the CLIPP of Fig. 1(a) can be scaled down by a factor of 10, corresponding to less than 30 µm overall length, at the price of an access frequency f_e of 100 MHz (due to a 10× increase of G and a 10× decrease of C_A). This would make the CLIPP integrable inside Si microrings with radius of less than 15 µm (i.e., around 100 µm ring length), this being the typical size of low-energy Si microring modulators [10].

The main drawback of a higher f_e is the reduction of the SNR. In fact, moving from 1 to 100 MHz, a 10× reduction of the SNR is expected because the CLIPP signal is 10 times higher (due to the reduction of G), but the noise level is 100 times higher (because of the larger noise spectral density increasing with frequency [17]). In order to reduce f_e, a thinner SiO_2 layer (down to 600 nm) can be used as waveguide upper cladding so as to increase C_A and correspondingly reduce the noise bandwidth. Further, to compensate for the SNR reduction, parasitic paths in parallel to the waveguide or toward the substrate can be minimized, for instance by adopting an insulating substrate. Note that the SNR can be also improved by increasing the voltage V_e applied to the CLIPP, yet at the price of some more perturbation of the optical field [16].

These considerations show that the integration of the CLIPP inside ultrasmall resonators with a radius of less than 5 µm [24] would require a higher readout frequency (several hundreds of megahertz). In this case, it could be more convenient to place the CLIPP outside the resonator. However, also in this case, the CLIPP would have a significant advantage compared to conventional integrated detectors [10,24], because it can be placed directly on the output bus waveguide of the resonator and no additional tap waveguides would be needed for monitoring operations.

4. TUNING THE MICRORING RESONANT WAVELENGTH

Figure 3(a) shows the variations of conductance ΔG induced by the propagation of quasi-transverse electric (TE) polarized light in the resonator, measured by the CLIPP versus wavelength, when the thermal actuator is off (blue line), and then driven with voltage $V_h = 2, 3, 4$ V (red, green, and orange lines). The microring has a linewidth of 51 pm (6.4 GHz), free spectral range of 1.115 nm (139.2 GHz), and quality factor of about 30,000. Also, the corresponding optical power traveling in the resonator is provided on the rightmost vertical axis, as estimated from the conductance variations ΔG measured by the CLIPP [16]. A peak conductance change of about 0.4 nS is measured ($B_e = 1$ Hz), corresponding to a SNR of about 200. Any spurious conductance change due to thermal crosstalk effects between CLIPP and heater is negligible here, being more than one order of magnitude smaller than ΔG induced by light at the low power levels utilized in this work.

The effectiveness of the CLIPP to monitor the transfer function of the microring is exploited to automatically tune its resonant wavelength in order to overlap with that of an external laser [Fig. 3(b)]. The laser wavelength is initially redshifted with respect to that of the resonator by about 230 pm (4.5 times the ring linewidth), then while the heater voltage V_h is automatically and continuously increased to shift the resonant wavelength (red line), the CLIPP simultaneously monitors the optical intensity stored in the cavity (blue line). In order to track this variation, a faster CLIPP response was achieved by enlarging B_e to 100 Hz (noise level of 9 pS rms). The inset of Fig. 3(b) shows the CLIPP monitoring the microring resonant wavelength versus the voltage applied to the heater. The tuning process, here achieved in about 260 ms, terminates when the optical power measured by the CLIPP reaches its maximum value, here for $V_h = 3.2$ V, condition that occurs only when the resonator wavelength is aligned to that of the laser.

Actually, Fig. 3(b) shows that the intracavity optical power measured by the CLIPP increases and then slightly decreases beyond the point where voltage is no longer changed. The reason is that an open loop tuning procedure does not ensure bringing the microring exactly at resonance condition. In this experiment, we estimated a 6 pm residual wavelength shift, corresponding to about 10% of the resonator 3 dB linewidth. The main cause for this inaccuracy is the instability of the fiber to waveguide optical coupling at the waveguide input that, in our setup, introduces power fluctuations on the order of ± 0.2 dB on a time scale of a few hundreds of milliseconds. Moreover, some residual thermal drift contributes to reducing the tuning accuracy. In order to make the tuning procedure independent on power fluctuation and more robust against thermal drifts, feedback control and locking algorithms must be used, as described in Section 5.

5. LOCKING THE MICRORING RESONANT WAVELENGTH

Here, we demonstrate that the CLIPP can be exploited for feedback-controlling the microring by locking its resonant wavelength to that of an external laser. The CLIPP monitors the intracavity optical intensity and provides a feedback error signal to the thermal actuator to adjust the resonant wavelength of the microring. In particular, we employ a common dithering technique [7], according to which a small modulation signal is applied to the resonator and then, by mixing it with the modulated intracavity optical intensity measured by the CLIPP, an error signal is extracted and used to drive the feedback loop [as shown in the schematic of Fig. 2(a)].

A. Generation and Readout of the Error Signal

Figure 4(a) shows the optical intensity in the resonator measured by the CLIPP, here low-pass filtered, when a sinusoidal dithering signal with frequency $f_d = 160$ Hz and amplitude $V_d = 100$ mV is applied to the heater of the resonator, as in the schematic of Fig. 2(a). In addition, a 2 V bias is applied to the heater in order to have the resonant wavelength overlapped to that of the laser. Here, a detection bandwidth $B_e = 1$ kHz is used to measure the conductance variation ΔG. The CLIPP also monitors the corresponding error signal ε [Fig. 4(b), red line] by demodulating the resonant optical power at frequency
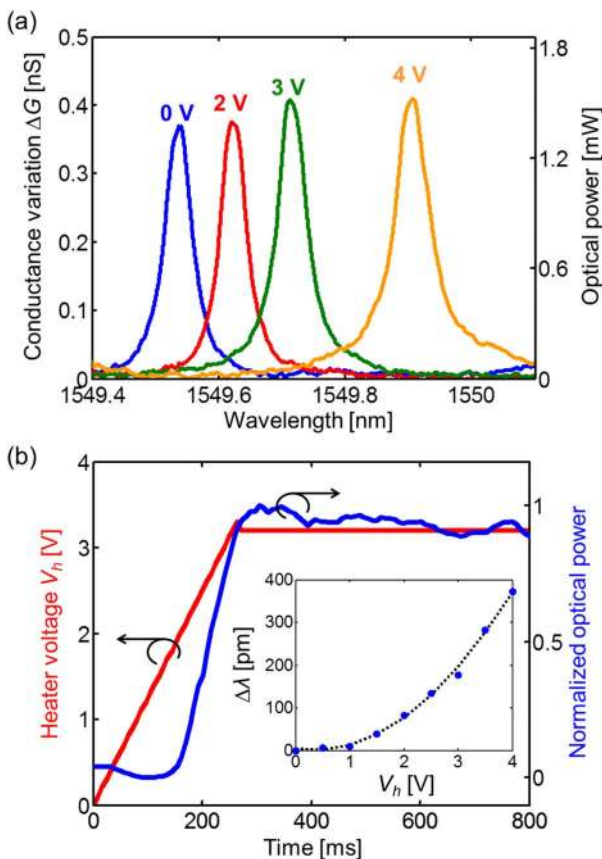

Fig. 3. Tuning of the microring resonant wavelength assisted by the CLIPP. (a) Light-induced conductance variation ΔG measured by the CLIPP ($B_e = 1$ Hz) and corresponding estimated optical power as a function of wavelength when the thermal actuator is off (blue line) and then switched on at $V_h = 2, 3, 4$ V (red, green, and orange lines). (b) Automated tuning of the resonator wavelength to that of an external laser, here detuned by about 230 pm, assisted by the CLIPP ($B_e = 100$ Hz); the inset shows the wavelength shift $\Delta\lambda$ measured by the CLIPP as the heater voltage V_h is increased from 0 to 4 V.
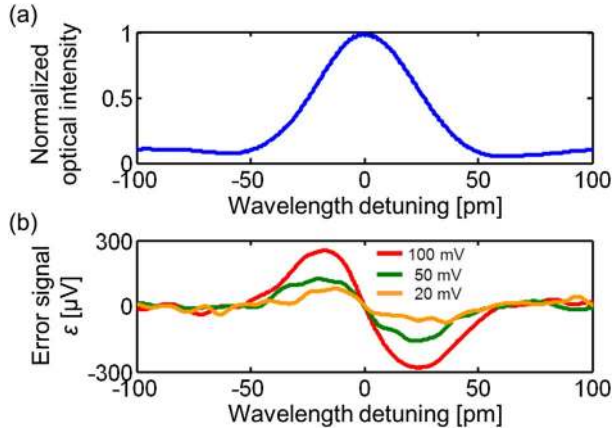
Fig. 4. Generation and readout of the error signal of the feedback-controlled microring. (a) Normalized optical intensity measured by the CLIPP versus wavelength, with $V_e = 1$ V and $f_e = 1$ MHz, when a dithering signal with amplitude $V_d = 100$ mV and frequency $f_d = 160$ Hz is applied to the heater. (b) Error signal ε extracted by the CLIPP by further demodulating the optical power P at the frequency of the dithering signal f_d for dithering amplitudes $V_d = 20$, 50, and 100 mV.

$f_e + f_d = 1.00016$ MHz. To extract the amplitude of the dithering signal applied to the heater, a second filter with a bandwidth $B_d = 100$ Hz is added, which ultimately sets the dominant time constant of the loop system (see Supplement 1). The error signal is zero at the resonant wavelength ($\lambda_r = 1549.54$ nm) and maximum on the slope of the resonator ($\lambda_r \pm 20$ pm). Also, thanks to the antisymmetric shape of ε, no ambiguity is left as to where λ_r is located. The application of a dithering signal with 100 mV amplitude corresponds to a thermal fluctuation as low as $\Delta T = 0.14$ K (wavelength shift $\Delta\lambda = 11$ pm, corresponding to about 20% of the linewidth) that is in line with those used for tap detectors [7] and does not affect the quality of the transmitted signal [10]. Though small, the amplitude of V_d can be further reduced to minimize the induced $\Delta\lambda$: in fact, with amplitudes of 50 mV and even 20 mV [Fig. 4(b), green and orange lines] corresponding respectively to $\Delta T = 0.07$ K ($\Delta\lambda = 5$ pm, 10% of the linewidth) and $\Delta T = 0.03$ K ($\Delta\lambda = 2$ pm, 4% of the linewidth), the error control signal is well above the noise level and can be used to drive the feedback loop.

B. Implementation of the Control Loop

In order to have the resonator wavelength λ_r continuously locked to that of an external laser λ_l, the CLIPP monitors simultaneously and continuously the intracavity optical intensity and the level of the error signal ε. As λ_r and λ_l drift apart from each other, the resonant optical power drops and the error signal deviates from zero. Consequently, the voltage applied to the heater is updated with an increment proportional to ε, its sign indicating the direction to follow (heating or cooling), and thus restoring the alignment between λ_r and λ_l.

The feedback loop is implemented by means of an integral controller whose gain k depends on the magnitude of ε with

respect to the wavelength detuning $\Delta\lambda$ [Fig. 4(b)], and on the wavelength shift that the heater can achieve [inset of Fig. 3(b)]. According to our model, k should be sufficiently high to achieve fast response of the feedback loop but, at the same time, low enough to guarantee stability of the system (see Supplement 1 for details). As an example, considering that $\Delta\varepsilon/\Delta\lambda = 15$ µV/pm around the resonant wavelength when $V_d = 100$ mV, and that the heater shifts λ_r by about 95 pm/V around 2 V bias, a controller gain around $k = 10,000$ is sufficient to provide a loop response as low as 50 ms, while maintaining the system stability according to the Bode criterion. Here, the controller is implemented by means of a programmable digital platform (FPGA), thus allowing more speed and flexibility in setting the controller parameters with respect to computer-assisted architectures.

C. Testing the Control Loop

The feedback loop is here tested against external fluctuations of the laser wavelength. Figure 5 shows the optical intensity in the microring, measured by the CLIPP as a function of time, when
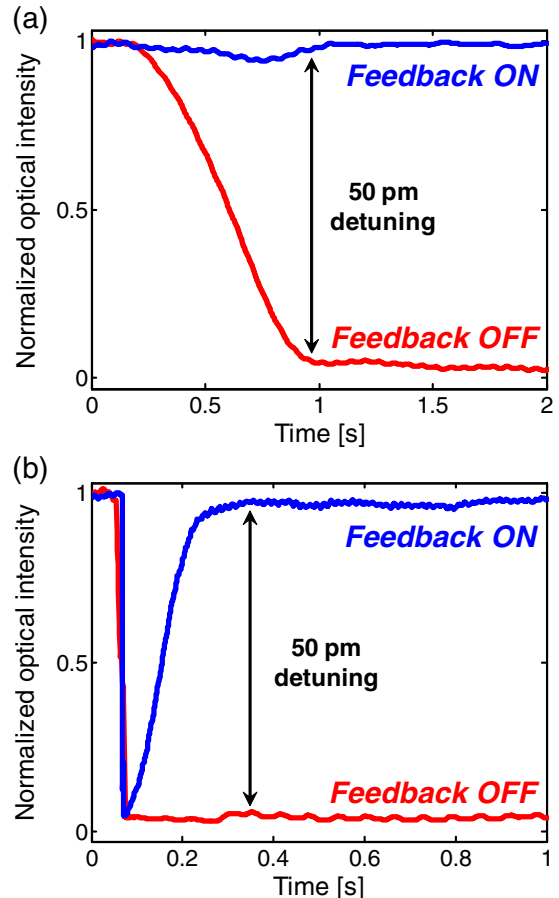

Fig. 5. Locking the microring resonant wavelength to that of an external laser λ_l assisted by the CLIPP. Normalized optical intensity in the resonator measured by the CLIPP when the feedback control is on (blue lines) and off (red lines) in the presence of (a) a continuous wavelength sweep (here occurring in about 700 ms) and (b) an instantaneous wavelength shift of the external laser by 50 pm (corresponding to 98% of the resonator linewidth). The considered 50 pm wavelength shift is the same of a temperature variation of 0.7 K.
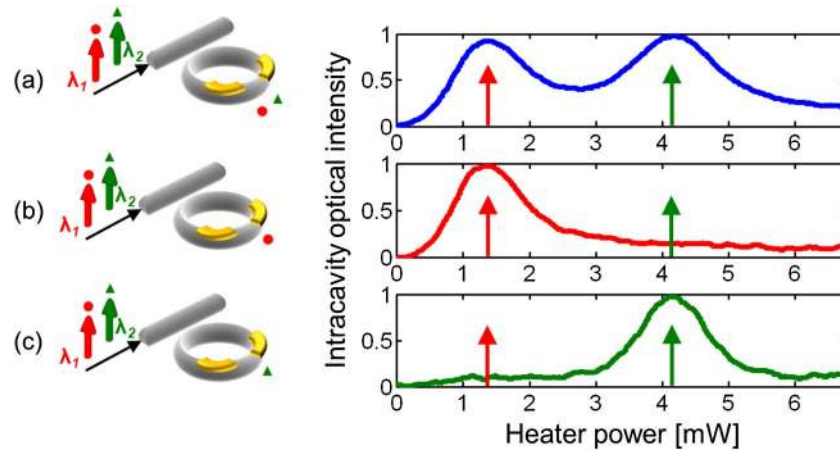
Fig. 6.   Swapping the resonator wavelength between two optical signals at wavelengths λ_1 (red arrow) and λ_2 (green arrow) injected in the microring. A weak modulation tone with depth 2% is added to label each of the optical carriers: the tone centered on λ_1 has frequency $f_1 = 10$ kHz (labeled with a red circle), whereas the tone around λ_2 has frequency $f_2 = 11$ kHz (labeled with a green triangle). The optical intensity measured by the CLIPP in the resonator is reported as a function of the electrical power dissipated on the heater when the CLIPP signal is demodulated at frequencies (a) $f_e = 1$ MHz, (b) $f_e + f_1 = 1.010$ MHz, and (c) $f_e + f_2 = 1.011$ MHz. When demodulating the CLIPP signal at frequency f_e, the signals λ_1 and λ_2 are indistinguishable; in constrast, when readout operations are performed at frequency $f_e + f_1$ ($f_e + f_2$), the CLIPP is able to identify distinctively λ_1 (λ_2).

the feedback routine is on (blue lines) and off (red lines), in presence of a detuning of λ_l by 50 pm, which is about the same as the resonator linewidth, and corresponding to a temperature variation of 0.7 K. In Fig. 5(a), where a continuous wavelength shift is imposed by the laser, no significant variation in the resonant optical intensity is observed (blue line) along the entire wavelength detuning (here occurring in about 700 ms). This means that λ_l and λ_r are always locked one to another by the feedback control. In these conditions, the closed-loop system works in the linearity range of the error signal of Fig. 4 (see Supplement 1 for details) and at the highest SNR condition ($B_d = 100$ Hz, noise level 9 pS rms, SNR > 40), because the CLIPP signal is always at its maximum [$\Delta G = 0.4$ nS, see Fig. 3(a)]. Actually, Fig. 5(b) shows that the feedback loop is able to bring the microring back to resonance even after an instantaneous wavelength shift of the laser source, thus making the control system work in less favorable conditions. As λ_l is abruptly changed by 50 pm, the optical intensity in the resonator drops to less than 5%, but then is rapidly restored (here in about 150 ms) to its initial level, where λ_l and λ_r overlap, by the feedback loop (blue line). Note that, although the SNR at 50 pm detuning is reduced to less than 5, the control system is still able to keep the microring locked. The beneficial effect of the feedback loop is confirmed when the control is switched off (red lines) in fact, in both cases, as λ_l shifts, the optical intensity in the resonator drops and is never compensated, having the laser wavelength completely outside of the resonator linewidth.

Although the speed of the control loop achieved here is well enough to counteract most of the drifts (thermal and others) experienced by Si photonic microrings, it can be significantly increased either with suitable control laws (such as proportional or proportional-integral) or by enlarging the CLIPP readout bandwidth. For instance, while keeping the current CLIPP bandwidth ($B_d = 100$ Hz), if a proportional controller

with gain of few thousands is utilized, a loop with time constant down to hundreds of microsecond is achieved (see Supplement 1 for details), yet at the price of larger voltage variations at the thermal actuator. On the other side, while maintaining an integral controller, the loop frequency can be increased by using a larger CLIPP bandwidth, yet at the price of larger noise (though typically depending on the square root of the bandwidth). The SNR can be preserved by increasing V_e accordingly.

6. SWAPPING THE MICRORING RESONANT WAVELENGTH

Although the CLIPP is in general a broadband light observer, here we show that it is able to simultaneously monitor and discriminate optical signals at different wavelengths. To this aim, we inject in the microring two different signals with wavelengths $\lambda_1 = 1549.59$ nm and $\lambda_2 = \lambda_1 + 120$ pm, labeled respectively with red and green arrows in Fig. 6. A weak modulation tone, with depth 2%, is added to label each of the optical carriers by means of an external modulator. The tone centered around λ_1 has frequency $f_1 = 10$ kHz whereas the other one, centered around λ_2, has frequency $f_2 = 11$ kHz (the tones are labeled, respectively, with red circle and green triangle in Fig. 6). The optical intensity observed in the resonator by the CLIPP is shown in Fig. 6 as a function of the electrical power dissipated by the heater. When the CLIPP electrical signal is demodulated at the usual frequency $f_e = 1$ MHz, the intracavity optical intensity reports two peaks associated with the transmission of both signals λ_1 and λ_2 [blue line in Fig. 6(a)] that are therefore indistinguishable. Vice versa, if the readout operations are performed at frequency $f_e + f_1 = 1.010$ MHz, the CLIPP is able to identify the signal at λ_1, where the modulation tone at frequency f_1 is added. In fact, as shown in Fig. 6(b) with the red line, the resonant peak measured by the CLIPP is centered on the first

signal (red arrow), whereas no evidence of λ_2 is found (green arrow). Similarly, if the electric signal is demodulated at frequency $f_e + f_2 = 1.011$ MHz, the measured resonant peak is centered on the second signal (green arrow), identified by the CLIPP as wavelength λ_2. It is straightforward now to tune and lock the microring resonant wavelength to that of the first signal λ_1 (λ_2), and then easily swap it to that of the second signal λ_2 (λ_1). Furthermore, it is worth noticing that wavelength-swapping operations can be performed by the CLIPP simultaneously on an arbitrarily large number of wavelengths using several modulation tones and by suitably demodulating the different signals. The same labeling approach can be used to manage many signals at the same wavelength but different light polarizations [16], or combined according to mode-division multiplexing schemes in multimode optical waveguides [25].

7. CONCLUSION

We have demonstrated non-invasive monitoring and advanced control functionalities in Si photonic microring resonators, assisted by a fully transparent light detector directly integrated inside the cavity. Through a CMOS microelectronic circuit [17] bridged to the Si photonic chip, the resonant wavelength of the microring is automatically tuned and locked against wavelength drifts of the optical signal. The non-invasive nature of the CLIPP enables real-time inspection of the intracavity light intensity without affecting the quality factor of the resonator. Therefore, the CLIPP can be used as a transparent detector for the realization of local feedback loops [14], thus making the control of devices integrated into complex circuits as if they were stand-alone.

Furthermore, the CLIPP is able to monitor and discriminate suitably labeled signals, allowing one to tune and lock photonic devices to the wavelength of a channel, regardless of the presence of other signals, simultaneously coexisting in the same photonic device. In the fabricated devices, feedback control is achieved through thermal actuators but the proposed tuning and locking schemes, and the CLIPP concept itself, can be adopted with any available actuator technology.

Finally, the possibility of managing feedback-controlled photonics through standard CMOS electronics makes the presented approach directly exploitable in system-level applications. The compactness and scalability of CMOS electronics to multichannel readout systems allows one also to extend the presented approach to the control of complex integrated circuits hosting many photonic components.

See Supplement 1 for supporting content.

REFERENCES

1. R. Chau, B. Doyle, S. Datta, J. Kavalieros, and K. Zhang, "Integrated nanoelectronics for the future," Nat. Mater. **6**, 810–812 (2007).
2. R. Gonzalez, B. M. Gordon, and M. A. Horowitz, "Supply and threshold voltage scaling for low power CMOS," IEEE J. Solid-State Circuits **32**, 1210–1216 (1997).
3. J. Sun, E. Timurdogan, A. Yaacobi, E. S. Hosseini, and M. R. Watts, "Large-scale nanophotonic phased array," Nature **493**, 195–199 (2013).
4. F. Morichetti, S. Grillanda, and A. Melloni, "Toward feedback-controlled integrated photonics," IEEE Photon. J. **6**, 1–6 (2014).
5. F. Xia, L. Sekaric, and Y. Vlasov, "Ultracompact optical buffers on a silicon chip," Nat. Photonics **1**, 65–71 (2007).
6. B. Guha, A. Gondarenko, and M. Lipson, "Minimizing temperature sensitivity of silicon Mach–Zehnder interferometers," Opt. Express **18**, 1879–1887 (2010).
7. K. Padmaraju, D. F. Logan, T. Shiraishi, J. J. Ackert, A. P. Knights, and K. Bergman, "Wavelength locking and thermally stabilizing microring resonators using dithering signals," J. Lightwave Technol. **32**, 505–512 (2014).
8. J. A. Cox, A. L. Lentine, D. C. Trotter, and A. L. Starbuck, "Control of integrated micro-resonator wavelength via balanced homodyne locking," Opt. Express **22**, 11279–11289 (2014).
9. K. Padmaraju, J. Chan, L. Chen, M. Lipson, and K. Bergman, "Thermal stabilization of a microring modulator using feedback control," Opt. Express **20**, 27999–28008 (2012).
10. K. Padmaraju, D. F. Logan, X. Zhu, J. J. Ackert, A. P. Knights, and K. Bergman, "Integrated thermal stabilization of a microring modulator," Opt. Express **21**, 14342–14350 (2013).
11. W. A. Zortman, A. L. Lentine, D. C. Trotter, and M. R. Watts, "Bit-error-rate monitoring for active wavelength control of resonant modulators," IEEE Micro **33**, 42–52 (2013).
12. T. Baehr-Jones, T. Pinguet, P. Lo Guo-Qiang, S. Danziger, D. Prather, and M. Hochberg, "Myths and rumours of silicon photonics," Nat. Photonics **6**, 206–208 (2012).
13. D. A. B. Miller, "Designing linear optical components," Opt. Photon. News **24**(12), 38 (2013).
14. D. A. B. Miller, "Self-configuring universal linear optical component," Photon. Res. **1**, 1–15 (2013).
15. J. K. Doylend and A. P. Knights, "The evolution of silicon photonics as an enabling technology for optical interconnection," Laser Photon. Rev. **6**, 504–525 (2012).
16. F. Morichetti, S. Grillanda, M. Carminati, G. Ferrari, M. Sampietro, M. J. Strain, M. Sorel, and A. Melloni, "Non-invasive on-chip light observation by contactless waveguide conductivity monitoring," IEEE J. Sel. Top. Quantum Electron. **20**, 1–10 (2014).
17. P. Ciccarella, M. Carminati, G. Ferrari, D. Bianchi, S. Grillanda, F. Morichetti, A. Melloni, and M. Sampietro are preparing a manuscript to be called "Impedance sensing CMOS chip for non-invasive light detection in integrated photonics."
18. M. Gnan, S. Thoms, D. S. Macintyre, R. M. De La Rue, and M. Sorel, "Fabrication of low-loss photonic wires in silicon-on-insulator using hydrogen silsesquioxane electron-beam resist," Electron. Lett. **44**, 115–116 (2008).
19. T. Baehr-Jones, M. Hochberg, and A. Scherer, "Photodetection in silicon beyond the band edge with surface states," Opt. Express **16**, 1659–1668 (2008).
20. W. Monch, *Semiconductor Surfaces and Interfaces* (Springer-Verlag, 2001).

21. H. Chen, X. Luo, and A. W. Poon, "Cavity-enhanced photocurrent generation by 1.55 μm wavelengths linear absorption in a p-i-n diode embedded silicon microring resonator," Appl. Phys. Lett. **95**, 171111 (2009).

22. J. D. B. Bradley, P. E. Jessop, and A. P. Knights, "Silicon waveguide integrated optical power monitor with enhanced sensitivity at 1550 nm," Appl. Phys. Lett. **86**, 241103 (2005).

23. M. W. Geis, S. J. Spector, M. E. Grein, R. T. Schulein, J. U. Yoon, D. M. Lennon, S. Deneault, F. Gan, F. X. Kaertner, and T. M. Lyszczarz, "CMOS-compatible all-Si high-speed waveguide photodiodes with high responsivity in near-infrared communication band," IEEE Photon. Technol. Lett. **19**, 152–154 (2007).

24. E. Timurdogan, C. M. Sorace-Agaskar, J. Sun, E. S. Hosseini, A. Biberman, and M. R. Watts, "An ultralow power athermal silicon modulator," Nat. Commun. **5**, 4008 (2014).

25. L. W. Luo, N. Ophir, C. P. Chen, L. H. Gabrielli, C. B. Poitras, K. Bergman, and M. Lipson, "WDM-compatible mode-division multiplexing on a silicon chip," Nat. Commun. **5**, 3069 (2014).